GROWTH OF SURFACE AND CORNER CRACKS IN BETA-PROCESSED AND MILL-ANNEALED Ti-6Al-4V

Paul D. Bell

Langley Research Center
Hampton, Va. 23665

NATIONAL AERONAUTICS AND SPACE ADMINISTRATION • WASHINGTON, D. C. • JULY 1975

1. Report No.	2. Government Accession No.	3. Recipient's Catalog No.
NASA TN D-7922		

4. Title and Subtitle	5. Report Date
GROWTH OF SURFACE AND CORNER CRACKS IN BETA-PROCESSED AND MILL-ANNEALED Ti-6Al-4V	July 1975
	6. Performing Organization Code
7. Author(s)	8. Performing Organization Report No.
Paul D. Bell	L-8864
	10. Work Unit No.
9. Performing Organization Name and Address	505-02-31-01
NASA Langley Research Center Hampton, Va. 23665	11. Contract or Grant No.
	13. Type of Report and Period Covered
12. Sponsoring Agency Name and Address	Technical Note
National Aeronautics and Space Administration Washington, D.C. 20546	14. Sponsoring Agency Code

15. Supplementary Notes

Author was a Langley/Industry Research associate and is now at Grumman Aerospace Corporation, Bethpage, New York.

16. Abstract

Empirical stress-intensity expressions were developed to relate the growth of cracks from corner flaws to the growth of cracks from surface flaws. An experimental program using beta-processed Ti-6Al-4V verified these expressions for stress ratios, $R \geqq 0$. An empirical crack growth-rate expression which included stress-ratio and stress-level effects was also developed.

Cracks grew approximately 10 percent faster in transverse-grain material than in longitudinal-grain material and at approximately the same rate in longitudinal-grain mill-annealed Ti-6Al-4V. Specimens having surface and corner cracks and made of longitudinal-grain, beta-processed material were tested with block loads. Increasing the stresses in a block did not significantly change the crack growth rates. Truncation of the basic ascending stress sequence within a block caused more rapid crack growth, whereas both the descending and low-to-high stress sequences slowed crack growth.

17. Key Words (Suggested by Author(s))	18. Distribution Statement
Crack growth Surface cracks Corner cracks Ti-6Al-4V	Unclassified – Unlimited New Subject Category 17

19. Security Classif. (of this report)	20. Security Classif. (of this page)	21. No. of Pages	22. Price*
Unclassified	Unclassified	32	$3.75

*For sale by the National Technical Information Service, Springfield, Virginia 22151

GROWTH OF SURFACE AND CORNER CRACKS IN BETA-PROCESSED AND MILL-ANNEALED Ti-6Al-4V

Paul D. Bell*
Langley Research Center

SUMMARY

Empirical stress-intensity expressions were developed to relate the growth of cracks from corner flaws to the growth of cracks from surface flaws. An experimental program using beta-processed Ti-6Al-4V verified these expressions for stress ratios, $R \geqq 0$. An empirical crack growth-rate expression which included stress-ratio and stress-level effects was also developed.

Cracks grew approximately 10 percent faster in transverse-grain material than in longitudinal-grain material and at approximately the same rate in longitudinal-grain mill-annealed Ti-6Al-4V. Specimens having surface and corner cracks and made of longitudinal-grain, beta-processed material were tested with block loads. Increasing the stresses in a block did not significantly change the crack growth rates. Truncation of the basic ascending stress sequence within a block caused more rapid crack growth, whereas both the descending and low-to-high stress sequences slowed crack growth.

INTRODUCTION

Failures of numerous aircraft and aerospace vehicle components have been traced to surface cracks. These cracks initiate at structural discontinuities such as holes, material defects, or other abrupt changes in cross section, and propagate to critical size at operating stress levels. In high-toughness materials and at stress levels below the yield stress of the material, surface cracks may propagate to through cracks before failure. However, in low-toughness (high-strength) materials, unexpected failures have been caused by small surface cracks. In designing against such failures, the designer must be able to predict the cyclic life required to propagate a small surface crack to failure under realistic aircraft loading.

---

*Langley/Industry Research Associate, now at Grumman Aerospace Corporation, Bethpage, New York.

This paper presents the results of fatigue-crack growth tests on specimens with either surface cracks, or surface cracks originating from the edge of circular holes (referred to as corner cracks). Beta-processed Ti-6Al-4V specimens were subjected to either constant-amplitude or programed loading. For constant-amplitude loading, the specimens were subjected to various maximum stress levels and stress ratios (ratio of minimum to maximum applied stress). The surface- and corner-crack specimens were also subjected to several sequences of block-programed loading. Mill-annealed Ti-6Al-4V specimens were also tested to determine whether this type of material processing affected fatigue-crack growth.

This paper also presents empirical stress-intensity expressions which are a function of surface-crack length, hole size, and plate width. These expressions were used to relate crack growth rates in surface- and corner-crack specimens.

SYMBOLS

The physical quantities in this paper are given in both the International System of Units (SI) and the U.S. Customary Units (ref. 1). The appendix presents factors relating these two systems of units.

a	surface-crack depth, m (in.)
B	one block of programed loading
C	empirical constant
c	surface-crack half-length or corner-crack length on front surface, m (in.)
$\frac{\Delta c}{\Delta N}$	rate of fatigue-crack growth in constant-amplitude tests, m/cycle (in/cycle)
$\frac{\Delta c}{\Delta B}$	rate of fatigue-crack growth in program-load tests, m/block (in/block)
K^*_{max}	maximum stress-intensity factor, $Nm^{-3/2}$ $\left(ksi\sqrt{in.}\right)$
ΔK^*	stress-intensity range, $Nm^{-3/2}$ $\left(ksi\sqrt{in.}\right)$
N	number of cycles
n,p,q	empirical constants

R	stress ratio, S_{min}/S_{max}
r	hole radius, m (in.)
ΔS	stress range, $S_{max} - S_{min}$, N/m^2 (ksi)
S_{max}	maximum gross stress, N/m^2 (ksi)
S_{min}	minimum gross stress, N/m^2 (ksi)
t	specimen thickness, m (in.)
W	specimen width, m (in.)
X, Y, Z	loading program designations
α	stress-intensity correction for finite specimen width
α_1	stress-intensity magnification factor for a through crack at edge of a hole
α_2	stress-intensity magnification factor for an eccentrically located through crack in a finite sheet
α_3	stress-intensity magnification factor which corrects for effect of hole on stress at edge of a finite sheet
β	combines stress-intensity magnification factors, $\alpha_1\alpha_2\alpha_3$

SPECIMEN PREPARATION

All beta-processed Ti-6Al-4V specimens were cut from a 19.8-mm-thick (0.78 in.) plate. (The tensile properties of this material are given in table I.) The longitudinal axes of all but two of these specimens paralleled the rolling direction of the plate. The longitudinal axes of the two exceptions were perpendicular to the rolling direction of the plate.

The mill-annealed Ti-6Al-4V specimens were cut from a 25.4-mm-thick (1.0 in.) plate. The longitudinal axes of all these specimens paralleled the rolling direction.

Figure 1(a) shows the configuration of the basic specimen blank. Figure 1(b) shows the details of the crack starter notches. A 0.76-mm-radius (0.030 in.) notch was machined on one surface of the surface-cracked specimens by electrical discharge. Corner-crack specimens were made by drilling a central, 12.7-mm-diameter (0.5 in.) hole through the specimen and then electrical-discharge machining a 0.76-mm-radius (0.030 in.) notch at the juncture of the hole wall and specimen surface.

To monitor crack growth, reference lines were scribed parallel to the loading direction on some crack-propagation specimens at a spacing of approximately 1.27 mm (0.050 in.). Wire crack-propagation gages having a wire spacing of 1.27 mm (0.050 in.) were applied to some of the specimens.

TESTING EQUIPMENT

A 1.33-MN (300 kip) closed-loop, servohydraulic testing machine (ref. 2) was used for all crack-propagation tests. Additional equipment included the following: a paper-tape programer for load control in the programed-load tests, a strip-chart recorder for a permanent load record during the programed-load tests, and an automatic crack-propagation detection system which was used during some of the tests. The crack-propagation detection system consisted of three basic components: crack-propagation gages, electronic system, and recording equipment. The crack-propagation gages, consisting of fine wires on a thin fiber backing, were bonded to the specimen surface. A small current was passed through the gages. When the crack in a specimen reached a given wire, the wire broke, changing the voltage across the gage. The electronic system sensed this change and actuated the recorder which recorded the new voltage, the number of applied cycles or blocks (supplied by the 1.33-MN hydraulic machine or the paper-tape programer), the specimen number, the date, and the time.

TEST PROCEDURES

Crack-propagation specimens were mounted in the test machine so that the center grip holes were loaded by matched-diameter bolts and by the clamping action of the grips. The specimens were first installed loosely in the grips; a tensile load of approximately 22 kN (5 kips) was applied to the specimens, and the grips were then tightened on the specimens. Tests demonstrated that the specimen did not slip in the grips when this procedure was used. A test on a center-crack specimen, fitted with four strain gages (one at each edge on each surface), demonstrated that this installation procedure produced a uniform stress throughout the test section. All tests were performed in a laboratory environment at approximately 295 K (72° F).

Constant-Amplitude Crack-Propagation Tests

The crack length was measured by one of three different methods. In the first method, the number of cycles required to propagate the crack to each scribe line was observed with a 25-power microscope and recorded. In the second method, the number of cycles required to reach predetermined crack lengths was recorded using a 25-power traveling microscope with an attached vernier scale; the vernier scale eliminated the need to scribe lines on the specimen. Crack-length increments as short as 0.1 mm (0.004 in.) could be measured with the vernier. In the third method, the number of cycles to break each wire on the crack-propagation gages was recorded automatically.

Generally, loads were applied to crack-propagation specimens at frequencies between 7 and 9 Hz, but frequencies were reduced to 1 to 2 Hz during visual measurements. Loads were monitored on an oscilloscope. The maximum error in the applied load was estimated to be less than 1 percent of the maximum applied load.

In some cases, the specimen was cycled at more than one load level to obtain faster crack initiation, or to acquire data on more than one stress level or stress ratio. In the case of specimens having a large $2a/W$ ratio and being subjected to compression loading, the tensile and compressive stress levels were equally reduced to keep the specimen from buckling.

Programed-Loading Tests

Programed-loading tests were conducted using the load programs shown in table II. The basic program for surface-crack specimens (designated Y-LH) represented a typical maneuver-critical aircraft spectrum. Program X-LH is the same as program Y-LH, except that all stress levels were increased by approximately 17 percent to test the effect of increased stress levels on crack growth rates. For corner-crack specimens all of the stress levels of program Y-LH were reduced by approximately 43 percent to prevent yielding of the material near the hole. The basic program for corner-crack specimens was designated Z-LH. Each of these programs consisted of five stress levels arranged in ascending (low-to-high) order. Six other programs were derived from the basic programs. In one of these six (Y-LHL) the stresses were arranged in a low-to-high-to-low sequence (i.e., LHL). For another (Y-HL), the stresses were arranged in a high-to-low sequence (H-L). In the remaining four the maximum stresses were truncated at either level 3 (Y-LH-3 and Z-LH-3) or level 4 (Y-LH-4 and Z-LH-4). In all programs, including the truncated versions, the total number of cycles per block was maintained at 1909. For all stress levels the minimum stress was zero. Loading frequencies ranged from 1 to 15 Hz. Loads were monitored periodically on an oscilloscope and errors were estimated to be less than ± 1 percent of the maximum value in each loading program. In addition, applied loads were recorded on a strip-chart recorder. Crack growth was

monitored by crack-propagation gages; the number of blocks of loading required to break each wire was recorded automatically.

Cracks were initiated at a stress ratio $R = 0$, and propagated to a length c of approximately 1.27 mm (0.05 in.) for both types of specimens before programed loads were applied. The initiation stress levels were 345 MN/m^2 (50.0 ksi) for surface-crack specimens and 275 MN/m^2 (39.9 ksi) for corner-crack specimens.

ANALYSIS

Specimens With Cracks Originating at Surface Flaws

A large part of the crack-propagation data were collected as the crack depth-to-thickness ratio approached unity or after the crack broke through the back surface of the specimen. Since the stress-intensity solutions for these configurations were not known, they were assumed to be through cracks; therefore, the equation for a through crack was used to calculate the stress-intensity range for these shapes. This equation has the form

$$\Delta K^* = \alpha \Delta S \sqrt{\pi c} \tag{1}$$

where c is the front-surface half-length, ΔS is the stress range, and α is the stress-intensity correction for a centrally located through crack in a finite-width plate. The α is given in reference 3 by

$$\alpha = \sqrt{\sec \frac{\pi c}{W}} \tag{2}$$

Equation (1) was assumed to be effective for all crack shapes ranging from small surface cracks to through cracks. The asterisk (*) was added to ΔK to prevent confusion with the literature.

Specimens With Cracks Originating at Corner Flaws

Most of the corner-crack data were gathered as the crack approached the back surface, or after the crack broke through this surface. Again, the stress-intensity solutions for these configurations are not known. Consequently, an approximate solution for ΔK was developed using Bowie's solution (ref. 4) for a through-the-thickness crack emanating from one edge of a circular hole in an infinite-width sheet. The Bowie solution is given by

$$\Delta K = \alpha_1 \Delta S \sqrt{\pi c} \tag{3}$$

where ΔS is the stress range, c is the front-surface crack length, and α_1 is the Bowie stress-intensity magnification factor. Values for α_1 are given in figure 3 of reference 4.

Two additional stress-intensity magnification factors were required to match equation (3) to the specimen configuration. One factor, the α_2, accounted for the finite width of the test specimens and was approximated by Isida's magnification factor (ref. 5) for an eccentrically located crack in a finite-width plate. In calculating the α_2, the effective length of the crack was assumed to be $2r + c$. The factor α_2 (from ref. 5) was approximated by

$$\alpha_2 = \sqrt{\sec\left(\frac{\pi}{2}\frac{2r + c}{W - c}\right)} \tag{4}$$

The other factor α_3 accounted for the interaction between the hole and the edge of the plate. Newman (ref. 6) showed that this interaction increased the stress-intensity factor by approximately 4 percent for the configurations used in this study. Consequently, α_3 was assumed to be 1.04.

The final equation used in calculating stress-intensity factors for the corner-flawed specimens is given by

$$\Delta K^* = \alpha_1\alpha_2\alpha_3\Delta S\sqrt{\pi c} = \beta\Delta S\sqrt{\pi c} \tag{5}$$

RESULTS AND DISCUSSION

Constant-Amplitude Tests

Crack-propagation test results for both the beta-processed and the mill-annealed materials are presented in table III. This table gives the number of cycles required to initiate the crack and to propagate it to the specified crack half-lengths (surface-crack specimens) or crack lengths (corner-crack specimens). In all cases the measured crack lengths were plotted against cycles and a smooth curve was faired through the data. The crack lengths and cycles from the faired curves were tabulated in tables III and IV and were used for all subsequent calculations. This procedure substantially reduced the scatter when crack growth rates were calculated.

Cracks originating at surface flaws.- Figures 2 to 4 show plots of $\Delta c/\Delta N$ against ΔK^* for the surface-crack specimens. For a given value of ΔK^*, crack growth rates increase as S_{max} decreases and also as R increases.

An equation of the form

$$\frac{\Delta c}{\Delta N} = C(1 + qR)^n(\Delta K^*)^n\left(S_{max}\alpha\right)^p \tag{6}$$

was fitted to the data in figures 2 to 4. Several values of q were assumed and then C, n, and p were calculated by a least squares analysis for each value of q. The following values gave the best fit to the data:

$$C = 8.62 \times 10^{-8} (5.15 \times 10^{-10})$$

$$n = 4.17$$

$$q = 0.8$$

$$p = -1.18$$

When C was calculated in SI units, ΔK^* is given in $MNm^{-3/2}$, S_{max} is given in MN/m^2, and $\Delta c/\Delta N$ is given in mm/cycle. When C was calculated in U.S. Customary Units, ΔK^* is given in ksi$\sqrt{\text{in.}}$, S_{max} is given in ksi, and $\Delta c/\Delta N$ is given in inch/cycle. The last term in equation (6) $(S_{max}\alpha)^p$ accounts for the stress-level effect on crack growth rates; this stress-level effect was apparent in figure 2.

In computing fatigue-crack growth rates for figures 2 to 4, the crack growth increment Δc was taken as the difference between successive crack lengths (usually 1.27 mm (0.05 in.)) from tables III and IV. The number of cycles of load required to propagate the crack through this increment was labeled ΔN. An average of the stress-intensity range values at the beginning and the end of each crack growth increment was used.

It is well known that crack-growth interaction effects may be present when the applied cyclic loading is modified. Since the investigation of these effects was not a part of this study, it was necessary to exclude some of the data gathered immediately after loads were changed. First, all of the crack growth-rate data obtained after the load change were plotted against the stress-intensity range. Then, if those data obtained immediately after the load change deviated significantly from the trend of the subsequent data, they were excluded from the analysis.

For data at $R = -1.0$ (figs. 3 and 4) the minimum stress was assumed to be zero when calculating the stress-intensity range. This assumption appears to be reasonable for this material since there is very little difference between the crack growth rates obtained at $R = -1$ and at $R = 0.02$.

Figure 5 shows the crack growth rate plotted against the stress-intensity range for the transverse- and longitudinal-grain specimens. Crack growth rates are approximately 10 percent slower in the transverse-grain specimens than in the longitudinal-grain specimens at the lower stress level. No significant difference was observed at the higher stress level.

Figure 6 shows the crack growth rate plotted against the stress-intensity range for both the mill-annealed and beta-processed specimens. For a given value of ΔK^*, cracks grew at essentially the same rates for the two conditions.

Cracks originating at corner flaws.- Cycles required to achieve various c for corner-crack specimens are presented in table III. Figures 7 to 9 show crack growth rate plotted against ΔK^* for the corner-crack specimens. These figures show that at a constant value of R and ΔK^*, the specimens which were cycled at lower maximum stresses exhibited faster crack growth rates than those cycled at higher maximum stresses. The figures also show that at a constant value of S_{max} and ΔK^*, the specimens cycled at a stress ratio of 0.5 exhibited faster crack growth rates than those cycled at a stress ratio of 0.02. For the specimens subjected to stress ratios less than zero, the minimum stress was assumed to be equal to zero whenever ΔK was calculated.

Equation (6) is plotted in figures 7 to 9 by using the empirical constants (i.e., C, q, n, and p) derived from the data on the surface-crack specimens and by substituting β for α in equation (6). Equation (6) fits the $R > 0$ corner-crack data quite well (figs. 7 and 8); the agreement indicates that the surface-crack data can be used to predict the crack growth in corner-crack specimens for $R \geq 0$. But equation (6) considerably underestimated the fatigue-crack growth rates for the $R = -1$ tests (fig. 9); perhaps the compressive portion of the loading cycle contributed more to the fatigue-crack growth in the corner-crack specimens than in surface-crack specimens.

Programed-Load Tests

Programed-load tests were conducted on both surface- and corner-crack specimens. The results of these tests are given in table IV. These data are presented in the same manner as the constant-amplitude data except that blocks of loads are substituted for cycles of loads. A block is defined as one complete load sequence totaling 1909 cycles. Two surface-crack specimens were tested using both the X-LH and Y-LH load programs. Figure 10 shows crack half-length plotted against blocks. It was expected that the specimens subjected to program X-LH would exhibit consistently faster crack growth rates than those subjected to program Y-LH, but figure 10 shows no consistent trend. At a given crack length and stress level, the stress in program X-LH produced higher values of ΔK^* than the stress in program Y-LH. However, the stress-level effect observed from the constant-amplitude data indicated that as the maximum stress was increased, the crack growth rate decreased. This effect may have been sufficient to offset the higher values of ΔK^* produced by the stresses in program X-LH. The Y-LH data were reduced and the crack growth per block was plotted against crack half-length (fig. 11). A scatter band was fitted around the data to facilitate subsequent comparisons.

Figure 12 shows a plot of a crack growth rate against crack half-length for the surface-crack specimens subjected to the truncated programs (Y-LH-3 and Y-LH-4). The scatter band for the data from load program Y-LH is also shown. A comparison of the scatter band with the data indicates that the crack growth rate was higher when the higher stress levels were truncated.

Figure 13 presents the crack growth rate plotted against the crack half-length for the specimens with the Y-HL and Y-LHL load programs. The data from the tests using either program exhibit somewhat slower growth rates than the Y-LH data. These rate relationships indicate that the Y-LH low-to-high loading sequence produced higher crack growth rates than the high-to-low loading sequence.

Figure 14 shows the crack growth rate plotted against the crack length for the corner-crack specimens. Load truncation caused higher rates of fatigue-crack growth.

CONCLUDING REMARKS

Both surface- and corner-crack specimens fabricated of beta-processed Ti-6Al-4V were tested with constant-amplitude or programed loads. A few surface-crack specimens, fabricated from transverse-grain beta-annealed material or from longitudinal-grain mill-annealed material, were also tested with constant amplitude loads. Approximate expressions were developed for stress-intensity factors for the surface- and corner-crack specimens. An empirical expression was developed to relate the crack growth rate to the approximate stress-intensity factors. Using this expression, the corner- and surface-crack data correlated well at positive stress ratios.

1. For a given value of stress-intensity range, (a) crack growth was faster at lower maximum stresses, and (b) crack growth was faster at higher stress ratios.

2. The crack growth in the transverse-grain beta-processed material was approximately 10 percent slower than in the longitudinal-grain beta-processed material.

3. The crack growth in the mill-annealed material was approximately the same as it was in the beta material.

4. The results of programed-load tests indicated that when all of the stresses within a block of loads were made larger by 17 percent the crack growth rates in surface-crack specimens did not change.

5. The specimens subjected to truncated loading programs exhibited faster crack growth than the specimens subjected to full loading programs.

6. Changing the basic load program from ascending stress levels to descending and low-high-low sequences produced slightly lower crack growth rates than those caused by a low-high sequence.

Langley Research Center,
National Aeronautics and Space Administration,
Hampton, Va., March 21, 1975.

APPENDIX

CONVERSION OF SI UNITS TO U.S. CUSTOMARY UNITS

The International System of Units (SI) was adopted by the Eleventh General Conference on Weights and Measures held in Paris in 1960 (ref. 1). Conversion factors required for units used herein are given in the following table:

Physical quantity	SI Unit (*)	Conversion factor (**)	U.S. Customary Unit
Force	newtons (N)	0.2248	lbf
Length	meters (m)	0.3937×10^{2}	in.
Stress	newtons per sq meter (N/m^2)	0.145×10^{-6}	ksi = 10^3 lbf/in^2
Stress intensity	newtons per $meter^{3/2}$ $(N/m^{3/2})$	0.9099×10^{-6}	$ksi\text{-}in^{1/2}$
Temperature	Kelvin (K)	(***)	^{o}F

*Prefixes to indicate multiple of units are as follows:

Prefix	Multiple
mega (M)	10^6
kilo (k)	10^3
milli (m)	10^{-3}

**Multiply value given in SI Unit by conversion factor to obtain equivalent in U.S. Customary Unit.

***Multiply value given in SI Unit by 1.8 and subtract 459.67 to obtain equivalent in U.S. Customary Unit.

REFERENCES

1. Anon.: Metric Practice Guide. E 380-72, Amer. Soc. Testing & Mater., June 1972.

2. Hudson, C. Michael; and Newman, J. C., Jr.: Effect of Specimen Thickness on Fatigue-Crack-Growth Behavior and Fracture Toughness of 7075-T6 and 7178-T6 Aluminum Alloys. NASA TN D-7173, 1973.

3. Brown, William F., Jr.; and Srawley, John E.: Plane Strain Crack Toughness Testing of High Strength Metallic Materials. Spec. Tech. Publ. No. 410, American Soc. Testing & Mater., c.1966.

4. Bowie, O. L.: Analysis of an Infinite Plate Containing Radial Cracks Originating at the Boundary of an Internal Circular Hole. J. Math. & Phys., vol. XXXV, no. 1, Apr. 1956, pp. 60-71.

5. Isida, M.: Stress-Intensity Factors for the Tension of an Eccentrically Cracked Strip. Trans. ASME, Ser. E: J. Appl. Mech., vol. 33, no. 3, Sept. 1966, pp. 674-675.

6. Newman, J. C., Jr.: An Improved Method of Collocation for the Stress Analysis of Cracked Plates With Various Shaped Boundaries. NASA TN D-6376, 1971.

TABLE I.- PHYSICAL PROPERTIES OF BETA-PROCESSED Ti-6Al-4V PLATE[a]

Ultimate tensile strength		Tensile yield strength		Modulus of elasticity		Elongation at failure,[b] percent
MN/m^2	ksi	MN/m^2	ksi	MN/m^2	ksi	
1053.8	152.8	987.6	143.1	122.1	17.7	13.8

[a]Average for 6 tests.

[b]50.8-mm (2.0 in.) gage length.

TABLE II.- LOAD PROGRAM DESCRIPTION

Program	Stress level	Maximum stress		Number of cycles
		MN/m^2	ksi	
X-LH	1	200.0	29.0	1240
	2	299.3	43.4	497
	3	399.3	57.9	141
	4	499.3	72.4	30
	5	599.3	86.9	1
Y-LH	1	171.0	24.8	1240
	2	255.9	37.1	497
	3	341.4	49.5	141
	4	426.9	61.9	30
	5	512.4	74.3	1
Y-LH-4	1	171.0	24.8	1240
	2	255.0	37.1	497
	3	341.4	49.5	141
	4	426.9	61.9	31
Y-LH-3	1	171.0	24.8	1240
	2	255.9	37.1	497
	3	341.4	49.5	172
Y-HL	1	512.4	74.3	1
	2	426.9	61.9	30
	3	341.4	49.5	141
	4	255.9	37.1	497
	5	171.0	24.8	1240
Y-LHL	1	171.0	24.8	620
	2	255.9	37.1	249
	3	341.4	49.5	71
	4	426.9	61.9	15
	5	512.4	74.3	1
	6	426.9	61.9	15
	7	341.4	49.5	70
	8	255.9	37.1	248
	9	171.0	24.8	620
Z-LH	1	114.5	16.6	1240
	2	171.7	24.9	497
	3	229.0	33.2	141
	4	286.2	41.5	30
	5	343.4	49.8	1
Z-LH-4	1	114.5	16.6	1240
	2	171.7	24.9	497
	3	229.0	33.2	141
	4	286.2	41.5	31
Z-LH-3	1	114.5	16.6	1240
	2	171.7	24.9	497
	3	229.0	33.2	172

TABLE III.- CONSTANT AMPLITUDE CYCLES REQUIRED TO REACH A SPECIFIED SURFACE CRACK LENGTH

Crack starter configuration	Condition	Grain direction	S_{max} MN/m²	S_{max} ksi	R	Number of cycles required to initiate and propagate a crack to a length c, mm (in.) of –																				
						1.27 (0.05)	2.54 (0.10)	3.81 (0.15)	5.08 (0.20)	6.35 (0.25)	7.62 (0.30)	8.89 (0.35)	10.16 (0.40)	11.43 (0.45)	12.70 (0.50)	13.97 (0.55)	15.24 (0.60)	16.51 (0.65)	17.78 (0.70)	19.05 (0.75)	20.32 (0.80)	21.59 (0.85)	22.86 (0.90)	24.13 (0.95)	25.40 (1.00)
Surface crack	Beta-processed	Longitudinal	480	69.6	0.02	14 370	20 300	22 720	23 850	24 530	25 000	25 330	25 580	25 750											
			[a]345	50.0	.02			27 700	91 000	92 900	104 900	105 630	106 250	106 720	107 100	107 380	107 590	107 740	107 850						
			[b]345	50.0	.02		217 300	223 900	227 100																
			205	29.7	.02					239 100	244 000	246 800	249 100	251 000	252 600	253 850	254 900	255 700	256 300	256 850	257 300	257 600	257 850	258 050	258 200
			480	69.6	.50				91 990	94 280	96 210	97 680	98 610	99 340	99 940	100 360	100 620	100 780	100 900	100 960					
			[c]345	50.0	.50		83 000	102 900	116 450	121 950	127 250	128 450	130 650	132 150	133 350	134 400	135 200	135 700	136 100	136 250					
			[d]345	50.0	-1.0		156 300	158 350	161 030	162 690	163 730	164 480	164 490												
			205	29.7	-1.0										169 300	169 810	170 310	170 800	171 210	171 610	171 970	172 290	172 590	172 810	173 480
			480	69.6	.02		15 700	18 030																	
			[e]345	50.0	.02				21 220	23 460															
			480	69.6	.02						24 520	24 920	25 100												
			[f]345	50.0	.25		94 700	104 500	109 650	112 250	114 050	115 300	116 250	117 050	117 650										
			345	50.0	.00											118 050	118 400	118 650	118 900	119 050	119 150				
		Transverse	480	69.6	0.02		14 190	16 260	17 540	18 350	18 810	19 160	19 415	19 580	19 690	19 770	19 825	19 860							
			345	50.0	.02	35 400	100 700	106 600	109 900	112 020	113 560	114 560	115 260	115 810	116 240										
	Mill-annealed	Longitudinal	480	69.6	0.02	18 350	24 200	26 700	28 200	28 870	29 280	29 550	29 730	29 870	29 960	30 040	30 100								
			480	69.6	.02	12 250	16 250	18 430	19 720	20 420	20 830	21 130	21 360	21 530	21 640	21 700									
			345	50.0	.02	15 100	35 130	40 900	44 100	45 900	47 100	47 950	48 550	49 000	49 400	49 630	49 830	49 930	50 030	50 100	50 150				
			345	50.0	.02	32 000	43 000	47 400	50 150	51 830	53 000	53 780	54 330	54 730	55 080	55 250	55 400	55 500	55 500	55 600	55 650	55 700			
Corner crack	Beta-processed	Longitudinal	480	69.6	0.02			1 950	2 210	2 405	2 545	2 660	2 745	2 810	2 860	2 900	2 933	2 963	2 990	3 010	3 033				
			380	55.1	.02	1 900	3 230	4 085	4 590	4 935	5 210	5 440	5 625	5 772	5 900	6 000	6 085	6 160	6 225	6 285	6 340	6 385	6 425		
			275	39.9	.02			10 570	11 660	12 560	13 350	13 480	14 500	14 950	15 320	15 640	15 800	16 130	16 340	16 550	16 720	16 850	16 970	17 050	17 130
			140	20.3	.02	52 000	89 200	102 300	111 200	117 700	123 000	127 400	131 200	134 500	137 400	139 800	141 900	143 900	145 800	147 500	149 200	150 800	152 100	153 400	154 300
			380	55.1	.50	3 950	8 260	10 720	12 450	13 720	14 900	15 850	16 700	17 400	18 000	18 450	19 020	19 450	19 800	20 100	20 350	20 600	20 800	20 990	21 150
			275	39.9	.50	19 700	27 350	32 100	35 650	38 600	41 100	43 300	45 200	46 850	48 450	49 850	51 200	52 350	53 400	54 350	55 200	56 050	56 750		
			140	20.3	.50	147 000	290 000	333 000	367 000	386 000	399 000	411 200	422 600	432 500	440 700	448 000	454 000	459 500	464 000	468 500	472 300	476 000	479 200	482 000	484 500
			140	20.3	.50	457 000	659 000	749 000	795 000	828 000	854 000	874 000	890 000	902 000	910 800	918 200	925 600	932 100	938 150	943 150	948 000	952 400	956 500	960 000	963 300
			[g]380	55.1	-1.0	122	706	1 009	1 026																
			[h]140	20.3	-1.0					30 000	31 500	32 700	33 750	35 150											
			140	20.3	.02										36 950	38 900	40 350	41 900	43 400	44 700	46 050	47 250	48 350	49 400	50 300

[a]Crack grown at 207 MN/m² (30.0 ksi) and R = 0.02 from c = 6.58 mm (0.259 in.) to 7.62 mm (0.300 in.) to mark crack front.

[b]Crack initiated using 345 MN/m² (50.0 ksi) and R = 0.02, for 227 590 cycles to c = 5.21 mm (0.205 in.)

[c]Crack initiated using 345 MN/m² (50.0 ksi) and R = 0.02 for 51 117 cycles.

[d]Stress reduced at 165 120 cycles and c = 10.62 mm (0.0418 in.) to prevent buckling of specimen.

[e]Crack grown at 345 MN/m² (50.0 ksi) and R = 0.02 from c = 3.96 mm (0.156 in.) to 8.10 mm (0.319 in.) to mark crack front.

[f]Stress ratio reduced to 0.00 at c = 12.95 mm (0.510 in.) and N = 117 720 cycles.

[g]Stress reduced at c = 5.05 mm (0.199 in.) and N = 1205 cycles to prevent buckling of specimen.

[h]Stress ratio increased at c = 11.43 mm (0.450 in.) and N = 35 150 cycles to prevent buckling of specimen.

TABLE IV.- PROGRAM LOAD CYCLES REQUIRED TO REACH A SPECIFIC SURFACE CRACK LENGTH

Crack starter configuration	Applied loading program	c at start of program loading		Number of blocks required to initiate and propagate a crack to a length c, mm (in.) of –																		
		mm	in.	1.27 (0.05)	2.54 (0.10)	3.81 (0.15)	5.08 (0.20)	6.35 (0.25)	7.62 (0.30)	8.89 (0.35)	10.16 (0.40)	11.43 (0.45)	12.70 (0.50)	13.97 (0.55)	15.34 (0.60)	16.51 (0.65)	17.78 (0.70)	19.05 (0.75)	20.32 (0.80)	21.59 (0.85)	22.86 (0.90)	24.13 (0.95)	25.40 (1.00)
Surface crack	A-LH	1.27	0.05	---	149	201	229	241	248	252	256	259											
	A-LH	1.65	.065	---	161	196	215	227	237	243	248												
	B-LH	1.42	.056	---	117	151	170	183	190	195	199	203	206										
	B-LH	1.32	.052	---	260	324	353	369	382	390	396	401											
	B-LH-4	1.45	.057	---	68	95	110	119.5	125	129	131.5	133.5	135	136	137	137.5	138						138
	B-LH-3	1.45	.057	---	55	82	93	99	102.5	105.5	108	110	111.5	113		114							
	B-H6	1.42	.056	---	134	224	276	297	311	320	328												
	B-LH6	1.40	.055	---	270.5	370.5	406.5	429.5	444.5	455.5	463.5	470.5	474.5	478	481.5								
Corner crack	C-LH	2.87	0.113	---		23	48	66	80	92	102	111	120	127	134	140	146	151	156	160	164	167	170
	C-LH	1.24	.049	2	24	44	63	79	94	107	117	127	136	144	152	159	165	171	176	180	184	187	190
	C-LH-4	1.22	.048	7	43	63	78	88	96	102	108	113	117	121	124	126	129	131	133	135	137	138	139
	C-LH-3	1.37	.054	---	24	38	47	53	58	62	66	69	72	74	77	79	80.5	82.5	84	86	87	88	89

Note: All specimens are beta-processed, longitudinal grain.

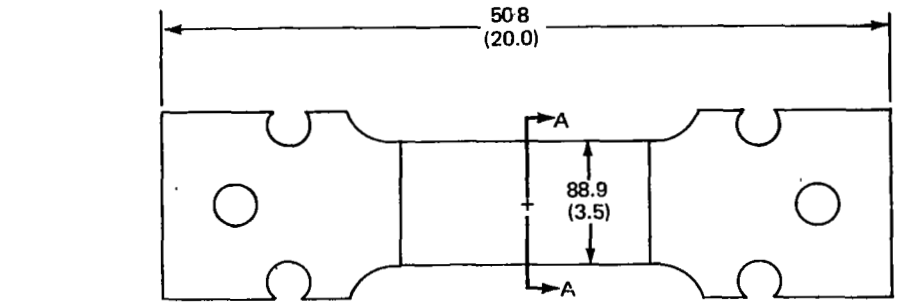

MATERIAL	t
BETA PROCESSED	19.8 (.78)
MILL ANNEALED	25.4 (1.00)

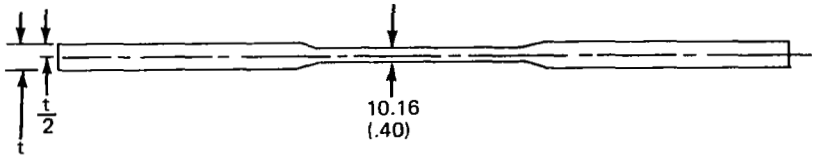

(a) Basic specimen blank.

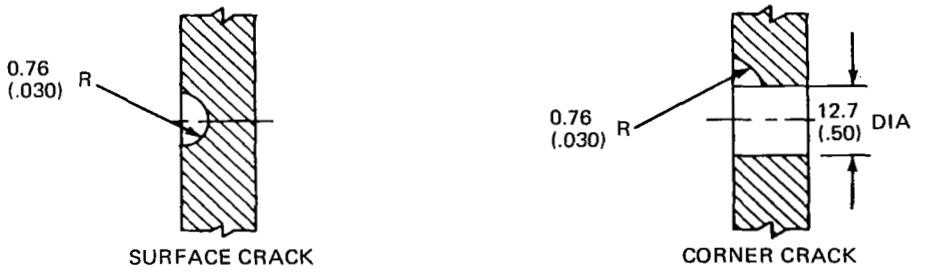

(b) Section A-A, starter notch details.

Figure 1.- Crack propagation specimen geometry.
All dimensions are given in mm (in.)

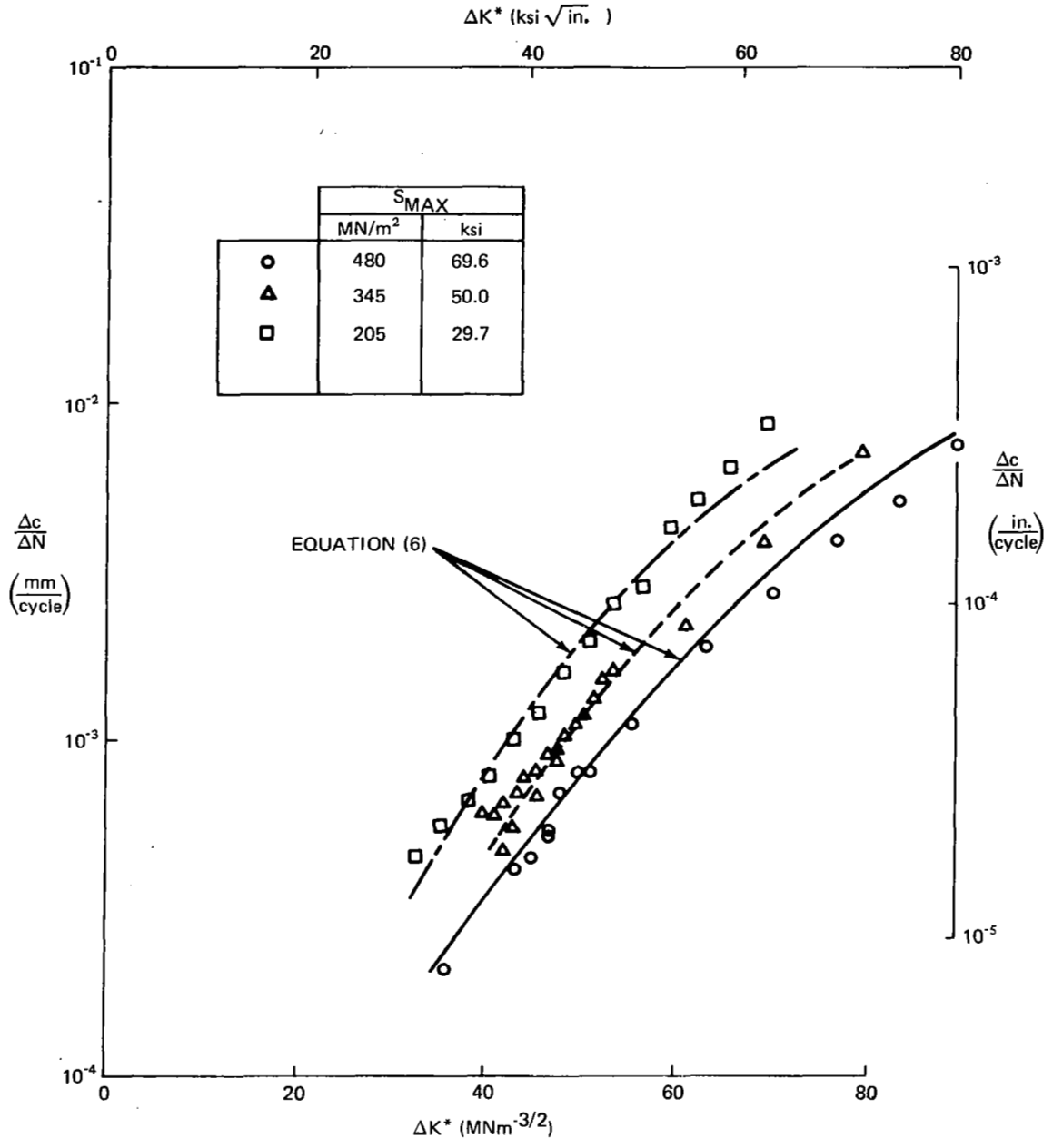

Figure 2.- Variation of fatigue crack growth rate with ΔK^*. Surface-flaw specimens. R = 0.02. Beta-processed. Longitudinal grain.

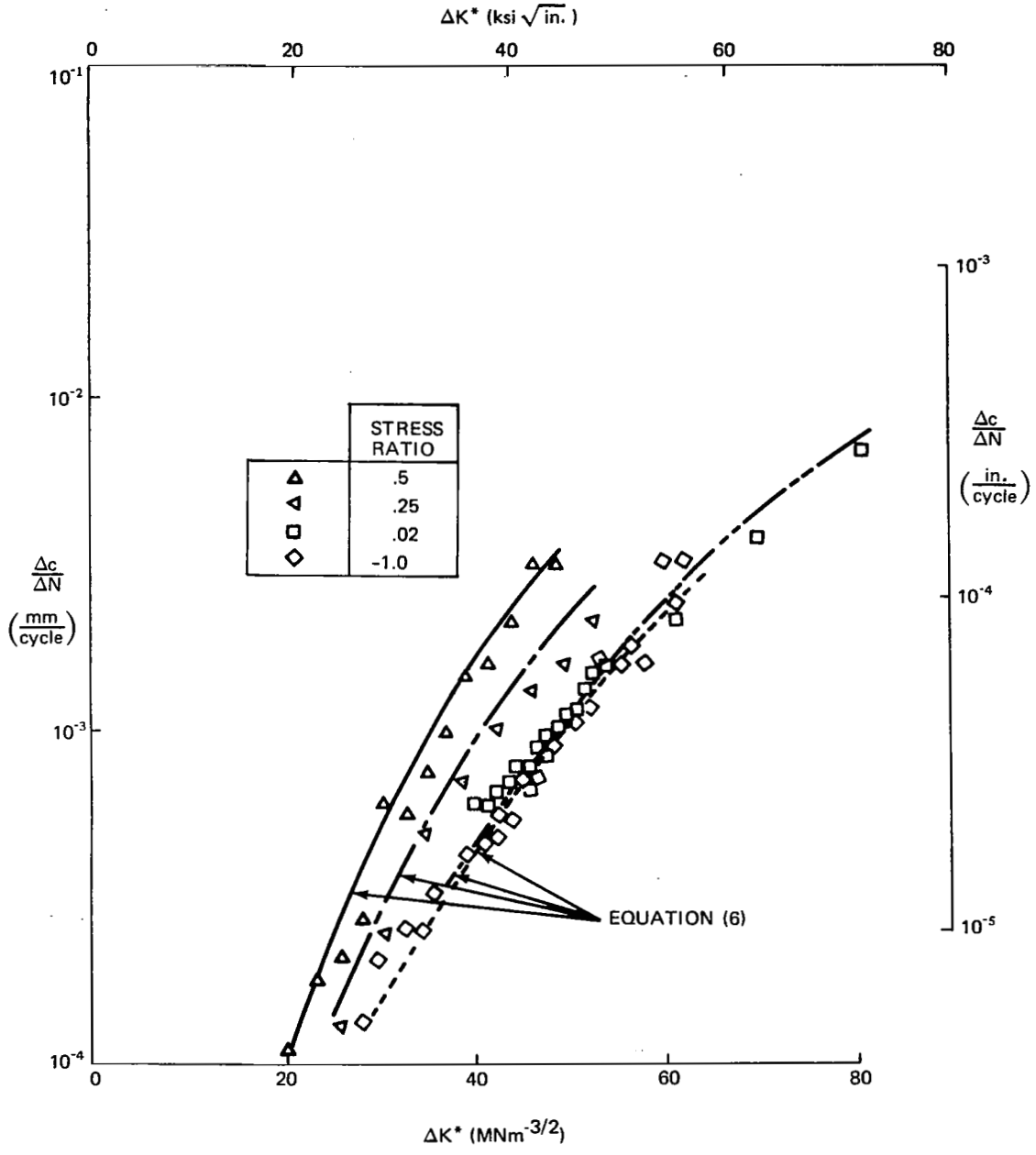

Figure 3.- Variation of fatigue crack growth rate with ΔK^*. Surface-flaw specimens. S_{max} = 345 MN/m^2 (50.0 ksi). Beta-processed. Longitudinal grain.

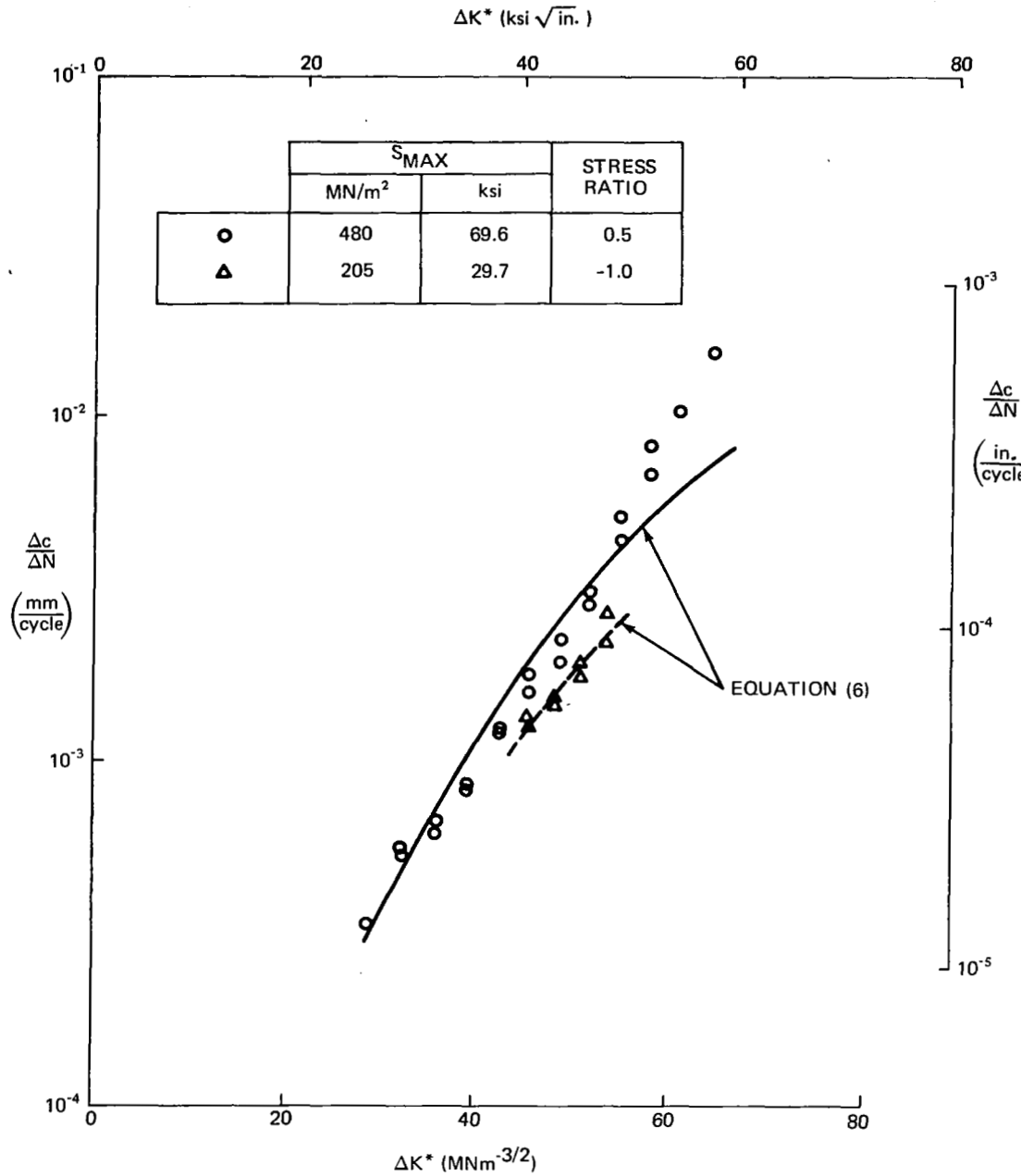

Figure 4.- Variation of fatigue crack growth rate with ΔK^*. Surface-flaw specimens. S_{max} = 480 MN/m^2 (69.6 ksi), R = 0.50 and S_{max} = 205 MN/m^2 (29.7 ksi), R = -1.0. Beta-processed. Longitudinal grain.

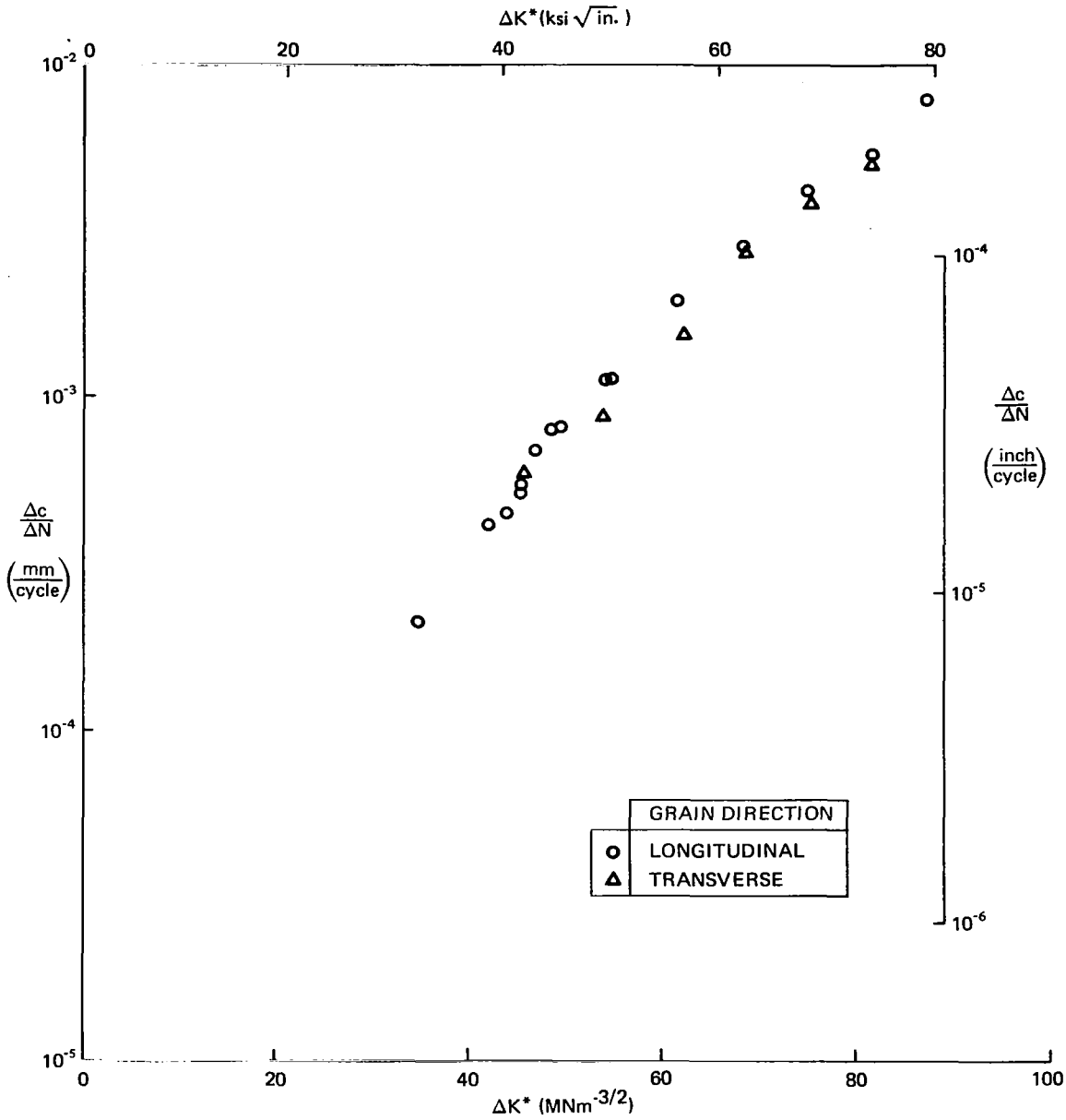

(a) S_{max} = 480 MN/m^2 (69.6 ksi).

Figure 5.- Variation of fatigue crack growth rate with ΔK^*. Surface-flaw specimens. R = 0.02. Beta-processed. Longitudinal and transverse grain.

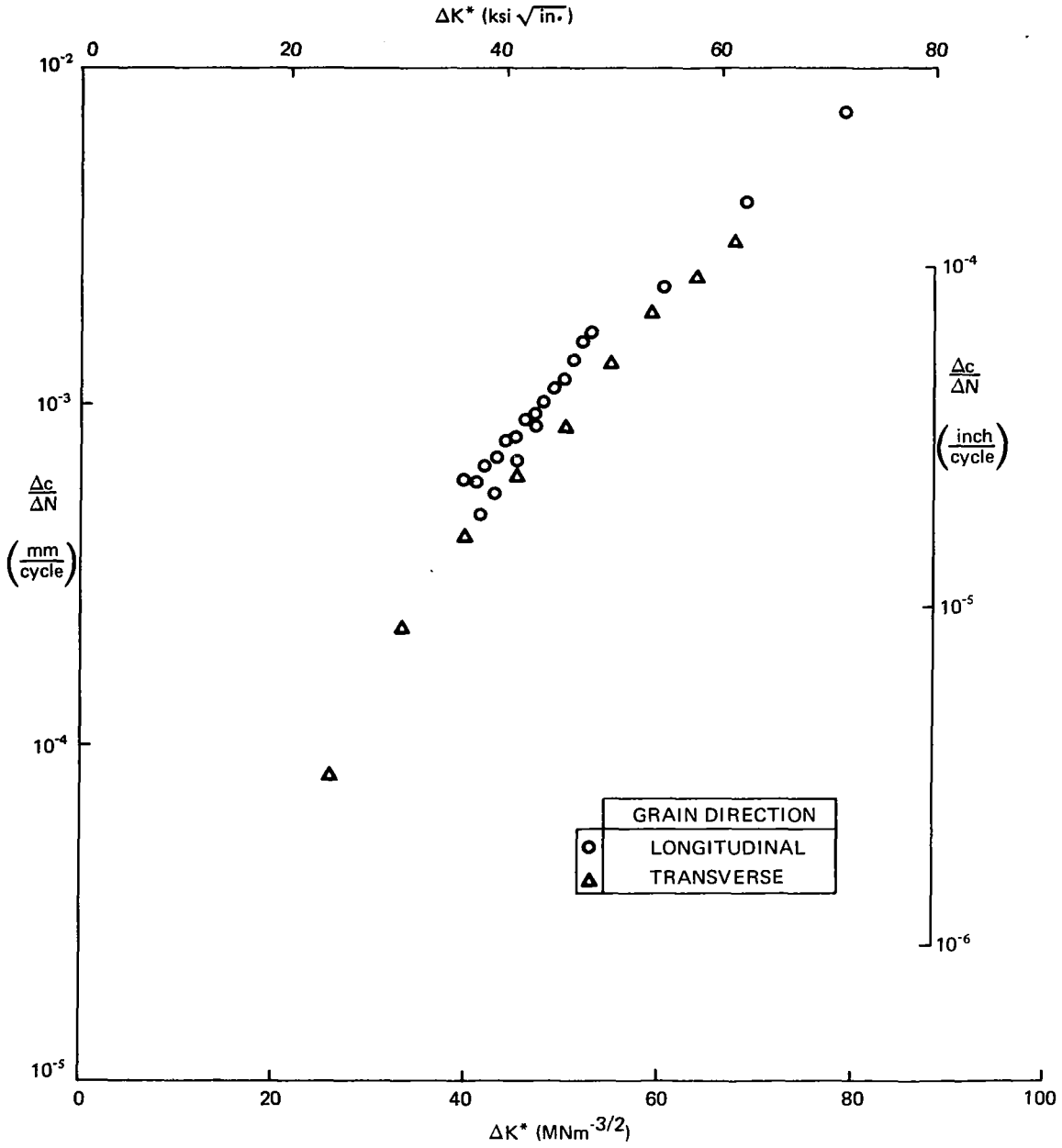

(b) S_{max} = 345 MN/m^2 (50.0 ksi).

Figure 5.- Concluded.

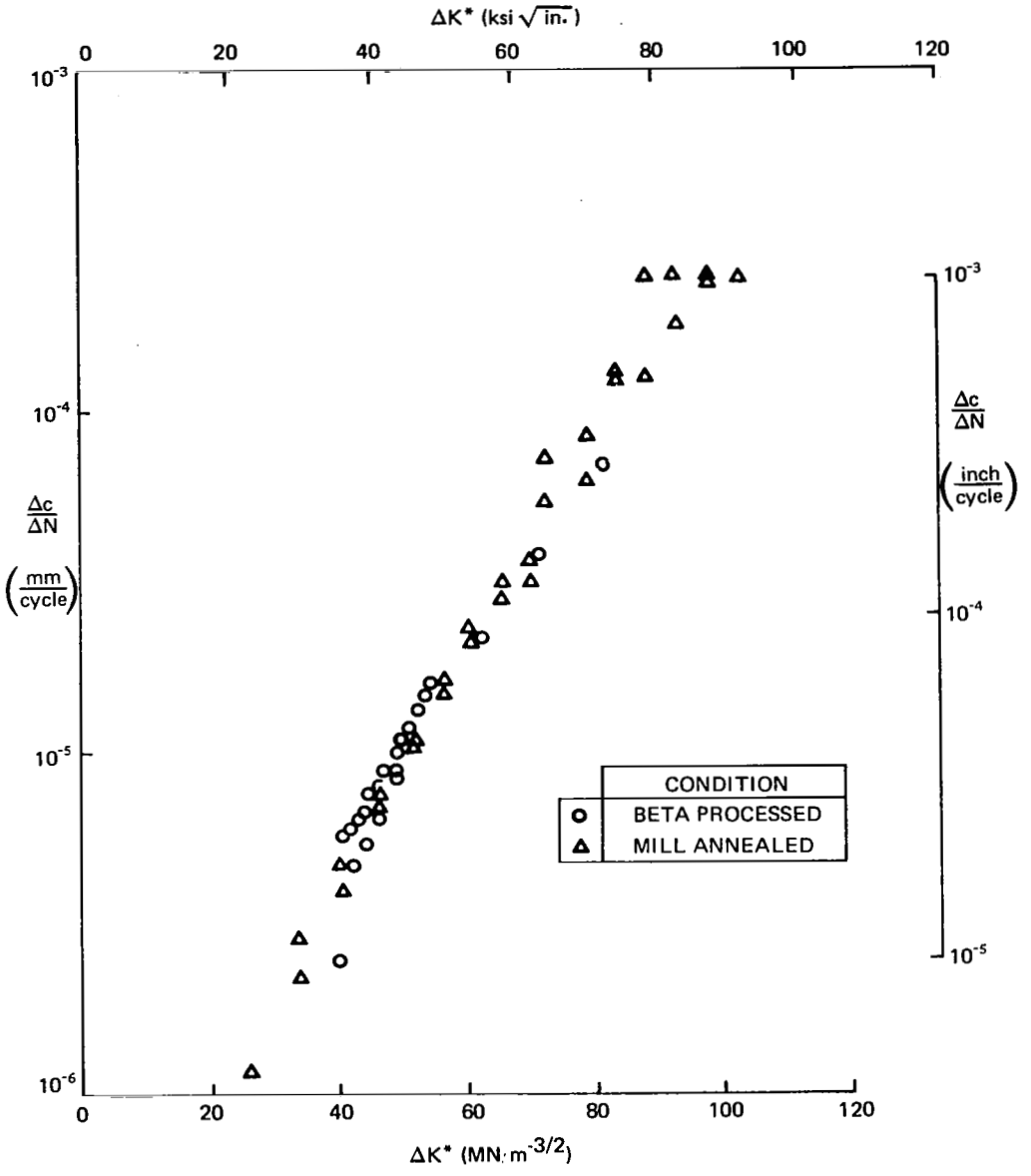

(a) S_{max} = 345 MN/m^2 (50.0 ksi).

Figure 6.- Variation of fatigue crack growth rate with ΔK*. Surface-flaw specimens. R = 0.02. Beta-processed and mill-annealed. Longitudinal grain.

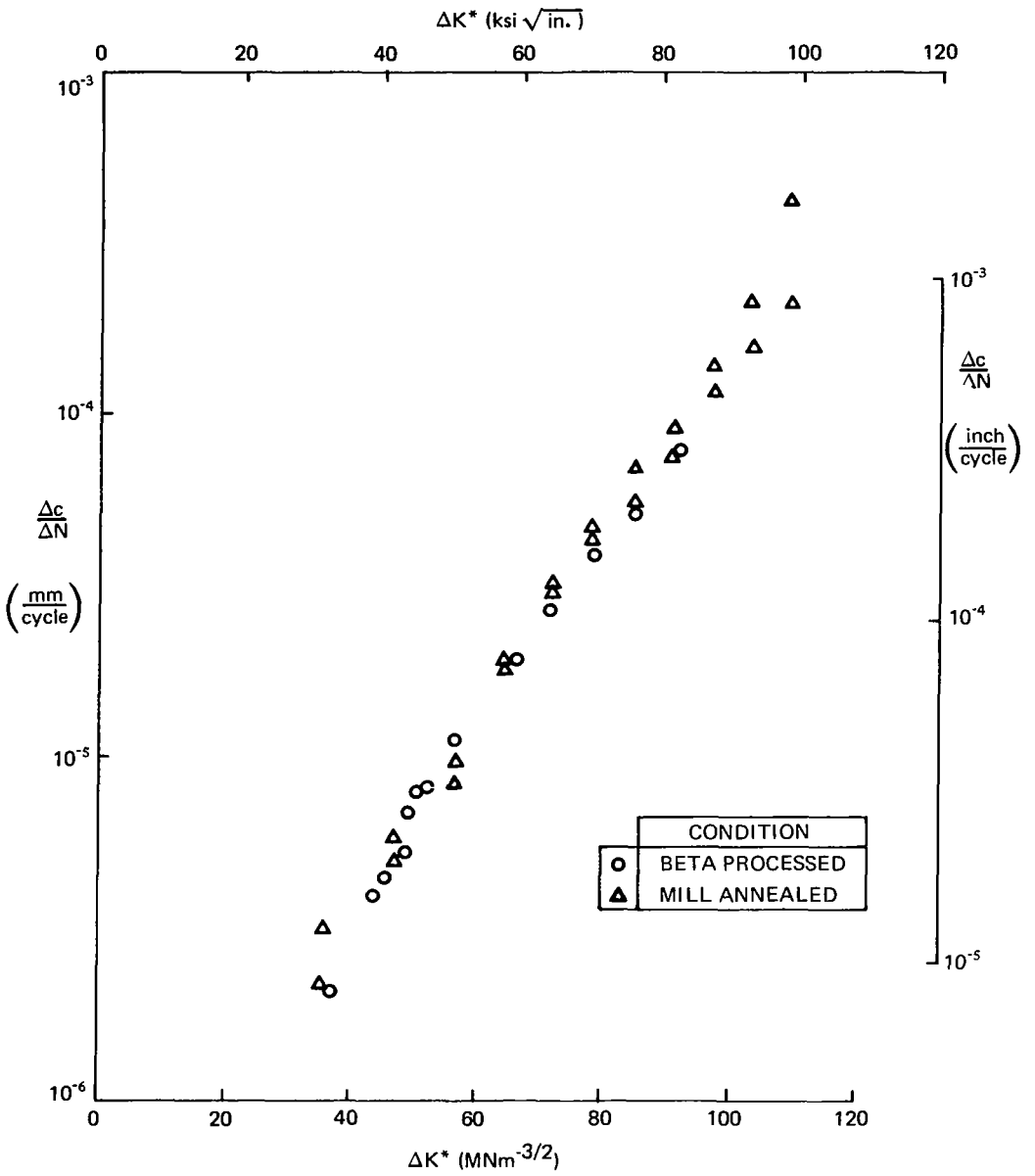

(b) S_{max} = 480 MN/m^2 (69.6 ksi).

Figure 6.- Concluded.

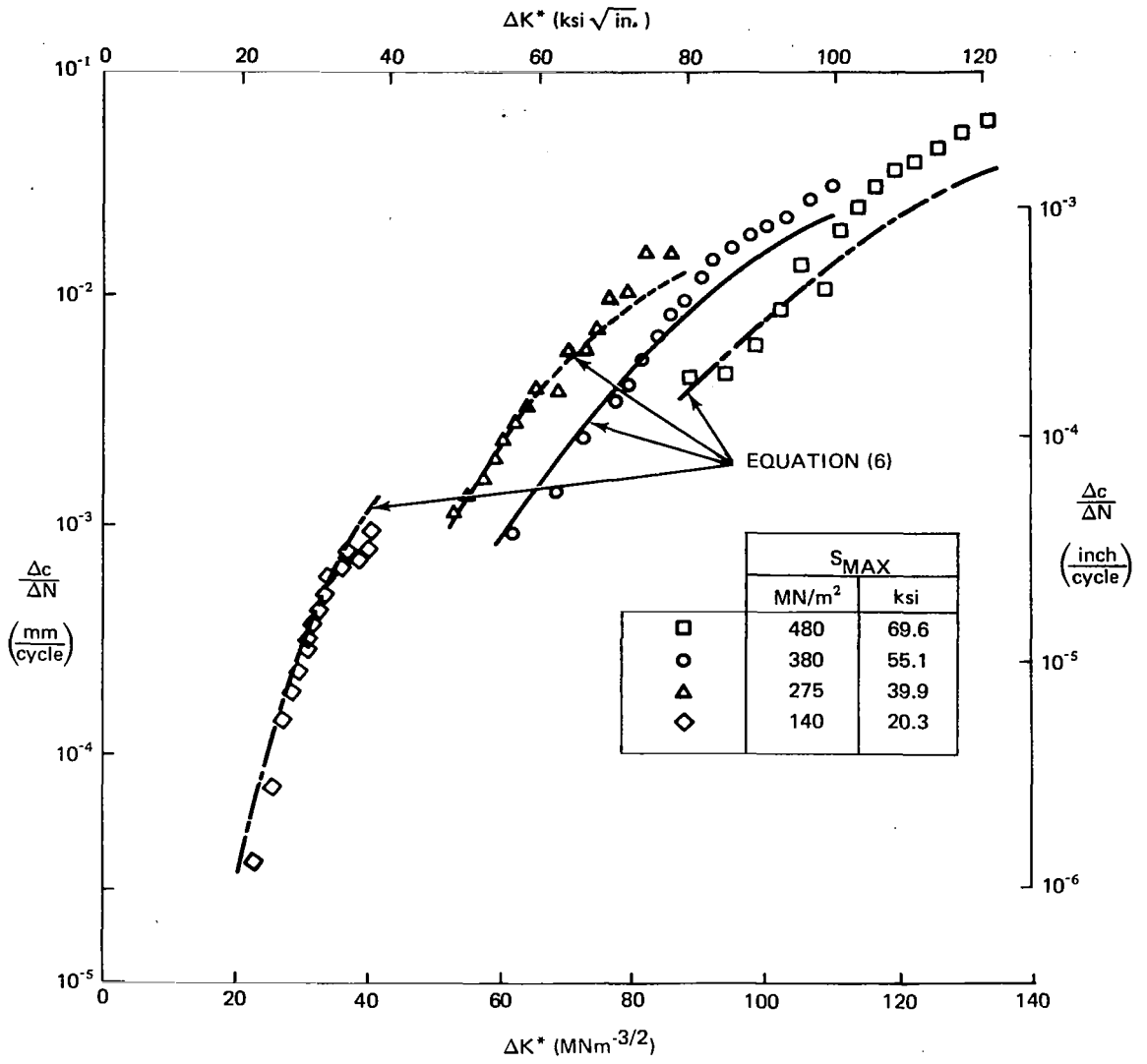

Figure 7.- Variation of fatigue crack growth rate with ΔK^*. Corner-flaw specimens. R = 0.02. Beta-processed. Longitudinal grain.

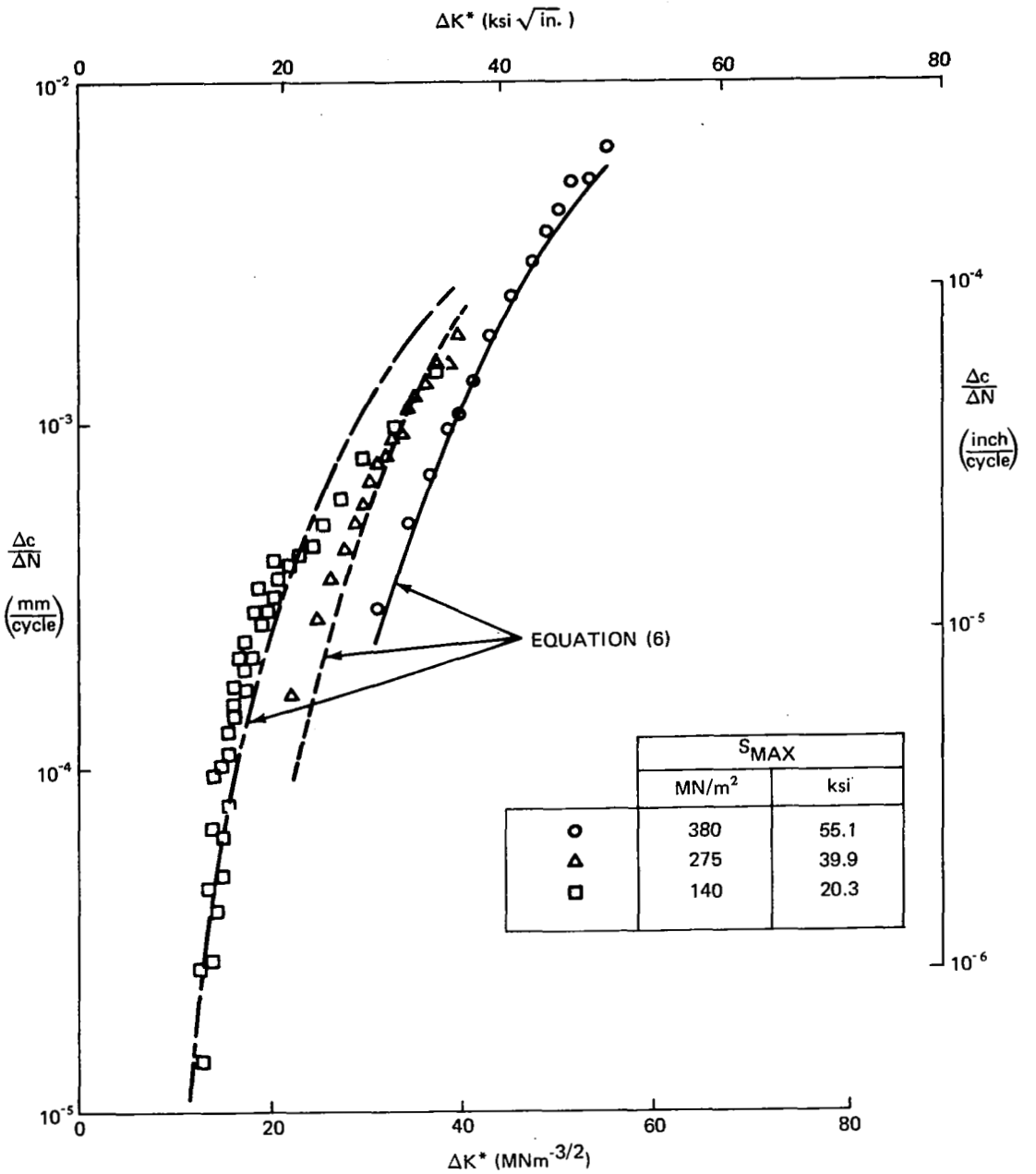

Figure 8.- Variation of fatigue crack growth rate with ΔK^*. Corner-flaw specimens. R = 0.50. Beta-processed. Longitudinal grain.

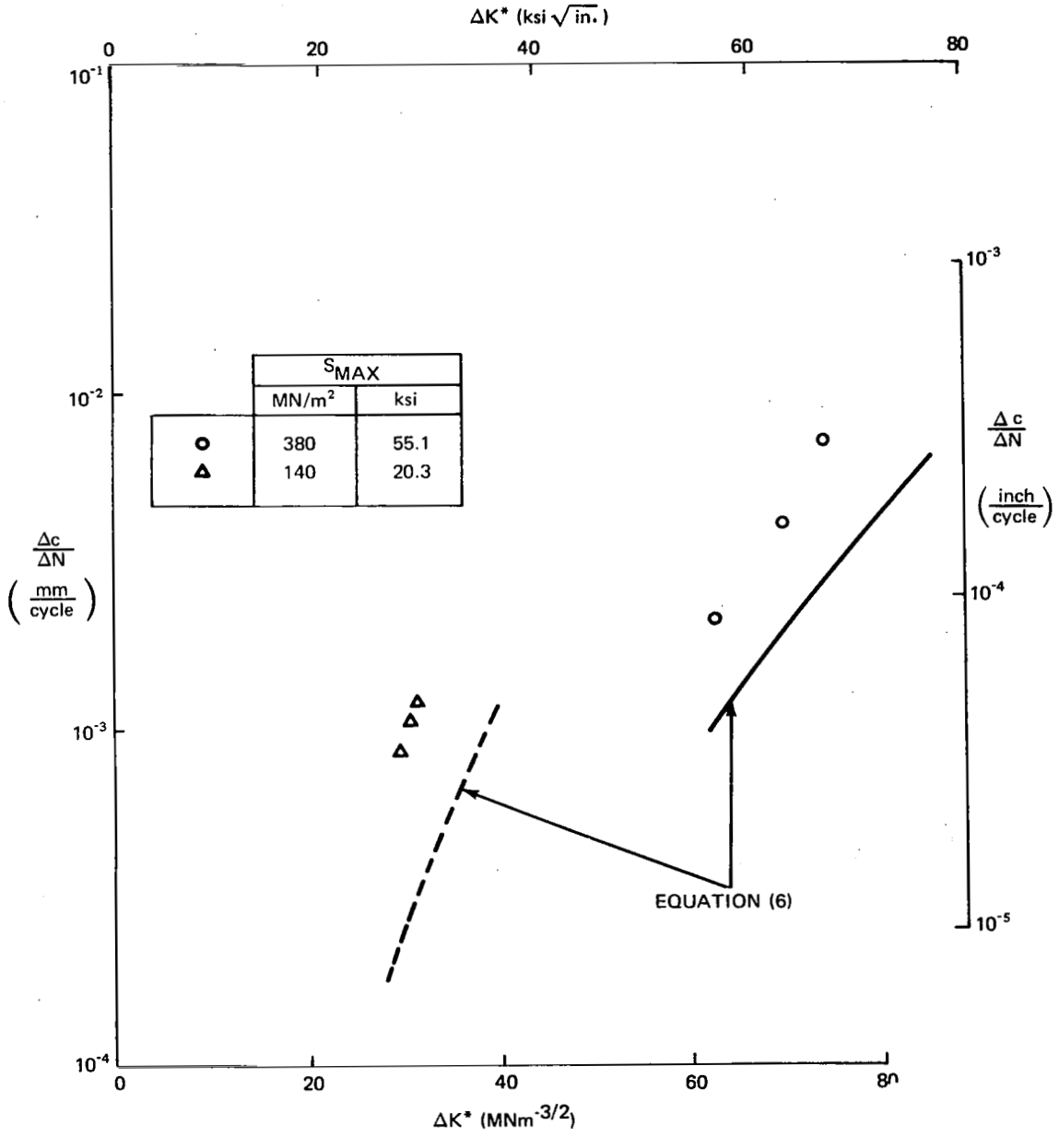

Figure 9.- Variation of fatigue crack growth rate with ΔK^*. Corner-flaw specimens. R = -1.0. Beta-processed. Longitudinal grain.

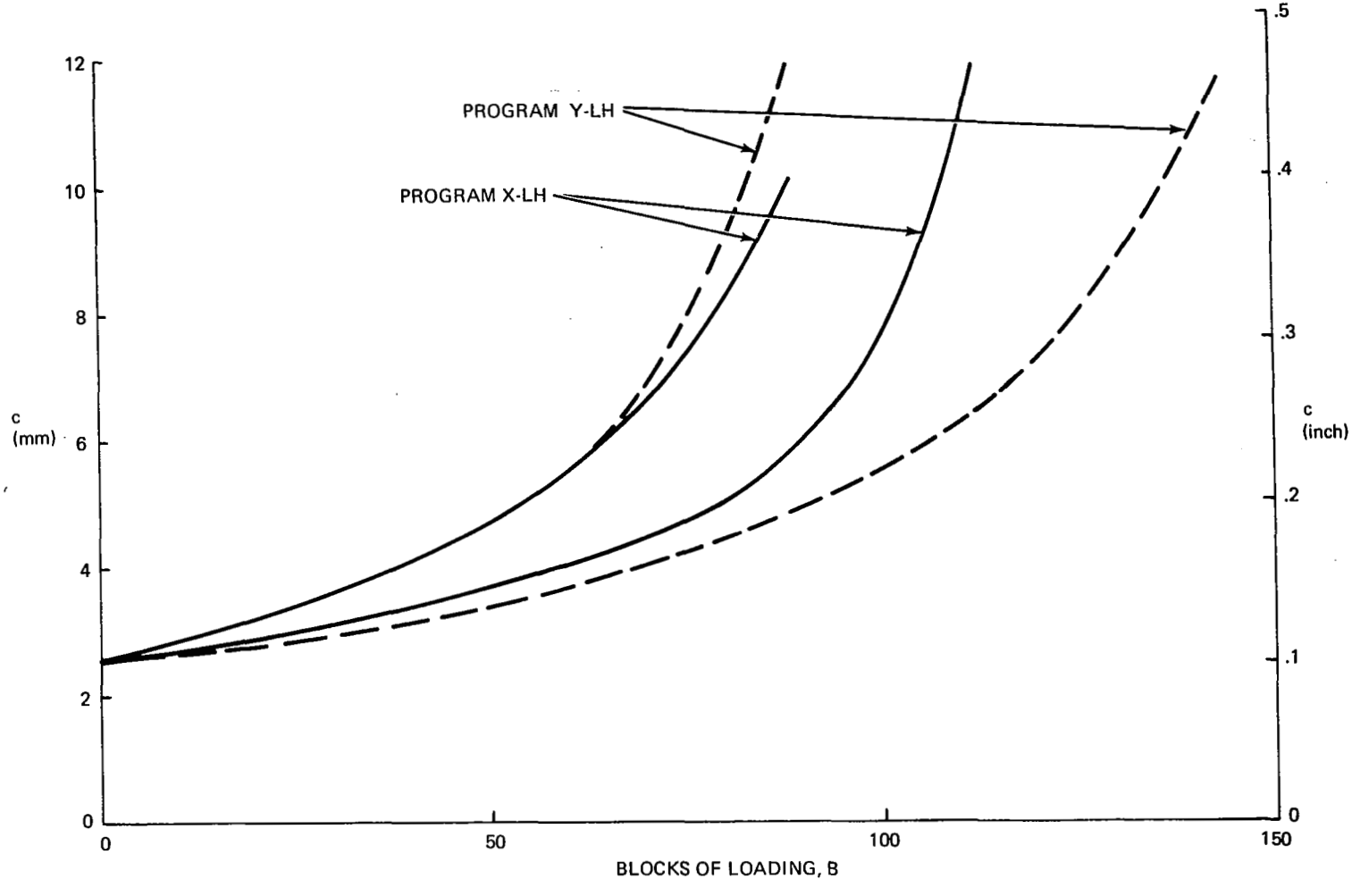

Figure 10.- Variation of half crack length with loading blocks. Surface-flaw specimens. Loading programs X-LH and Y-LH. Beta-processed. Longitudinal grain.

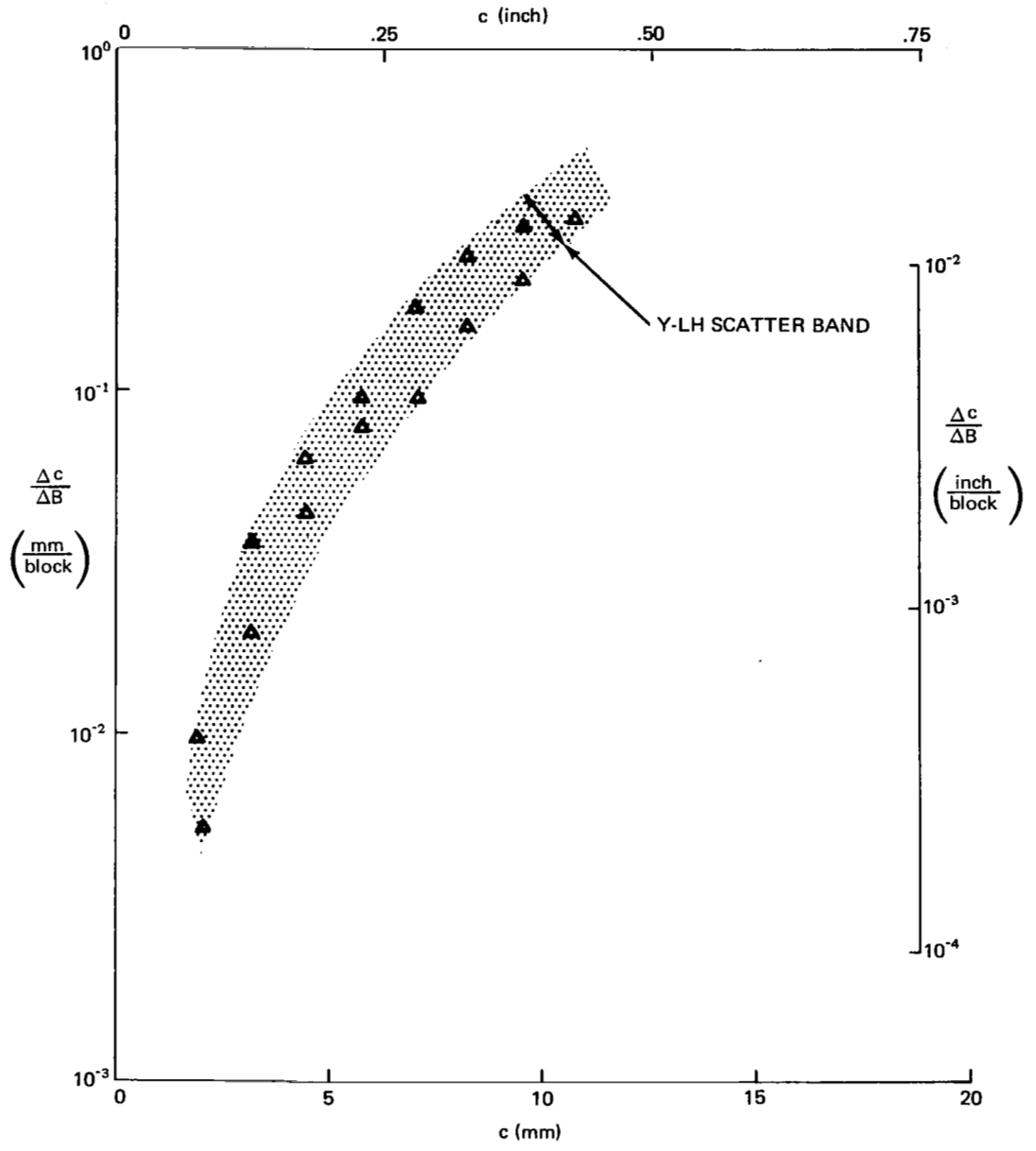

Figure 11.- Variation of fatigue crack growth rate with c. Surface-flaw specimens. Loading program Y-LH. Beta-processed. Longitudinal grain.

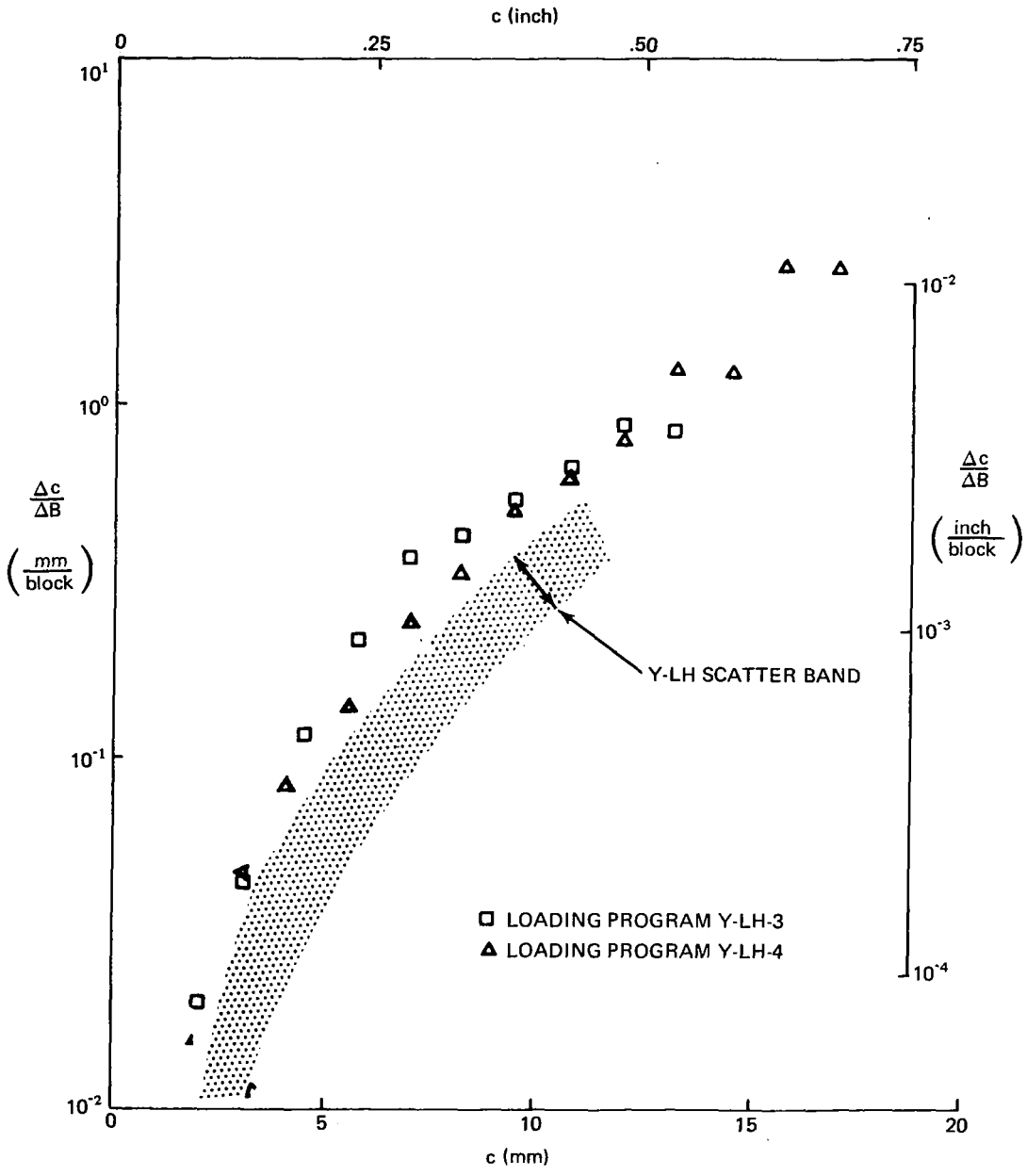

Figure 12.- Variation of fatigue growth rate with c. Surface-flaw specimens. Loading programs Y-LH-3 and Y-LH-4. Beta-processed. Longitudinal grain.

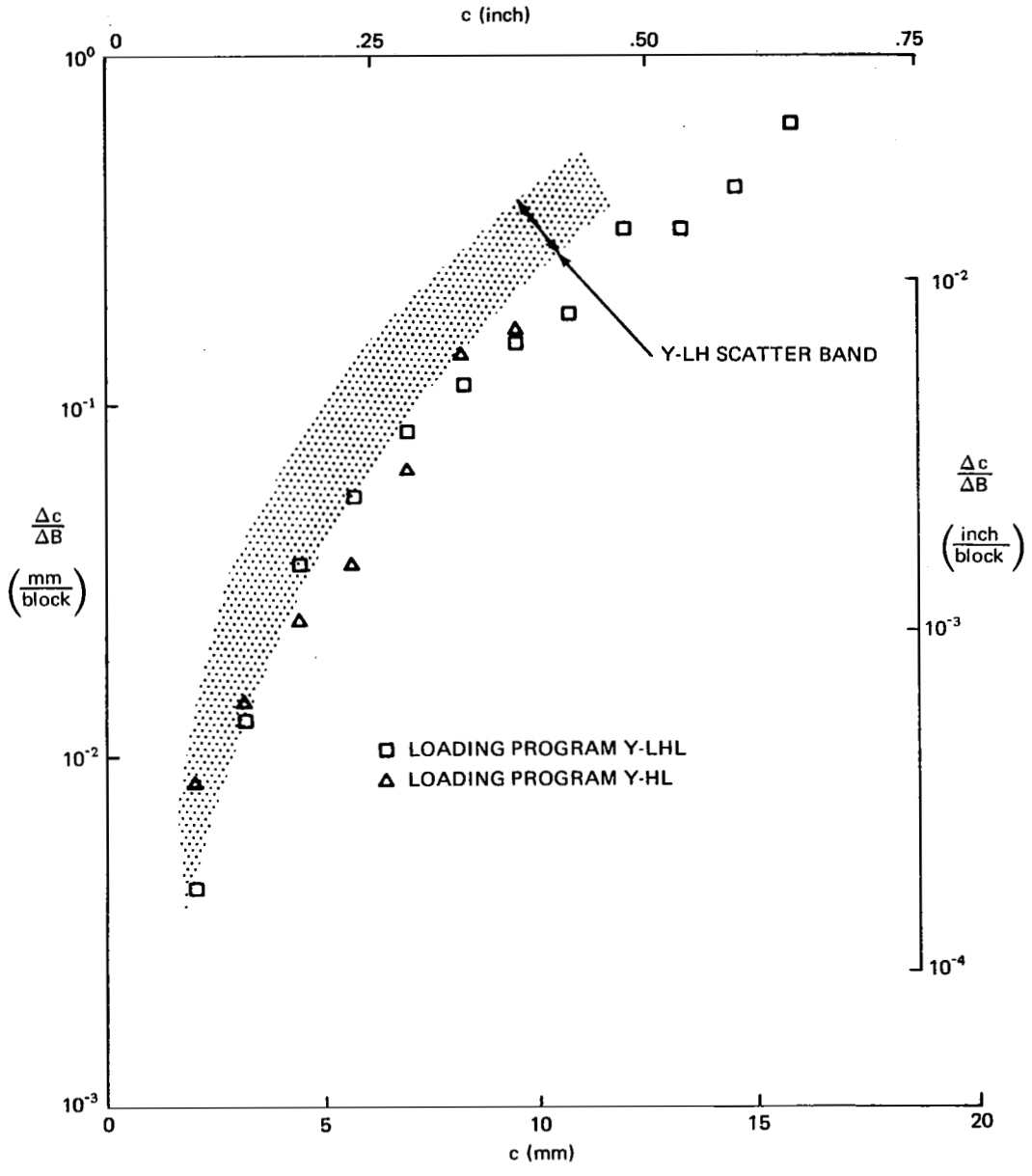

Figure 13.- Variation of fatigue crack growth rate with c. Surface-flaw specimens. Loading programs Y-HL and Y-LHL. Beta-processed. Longitudinal grain.

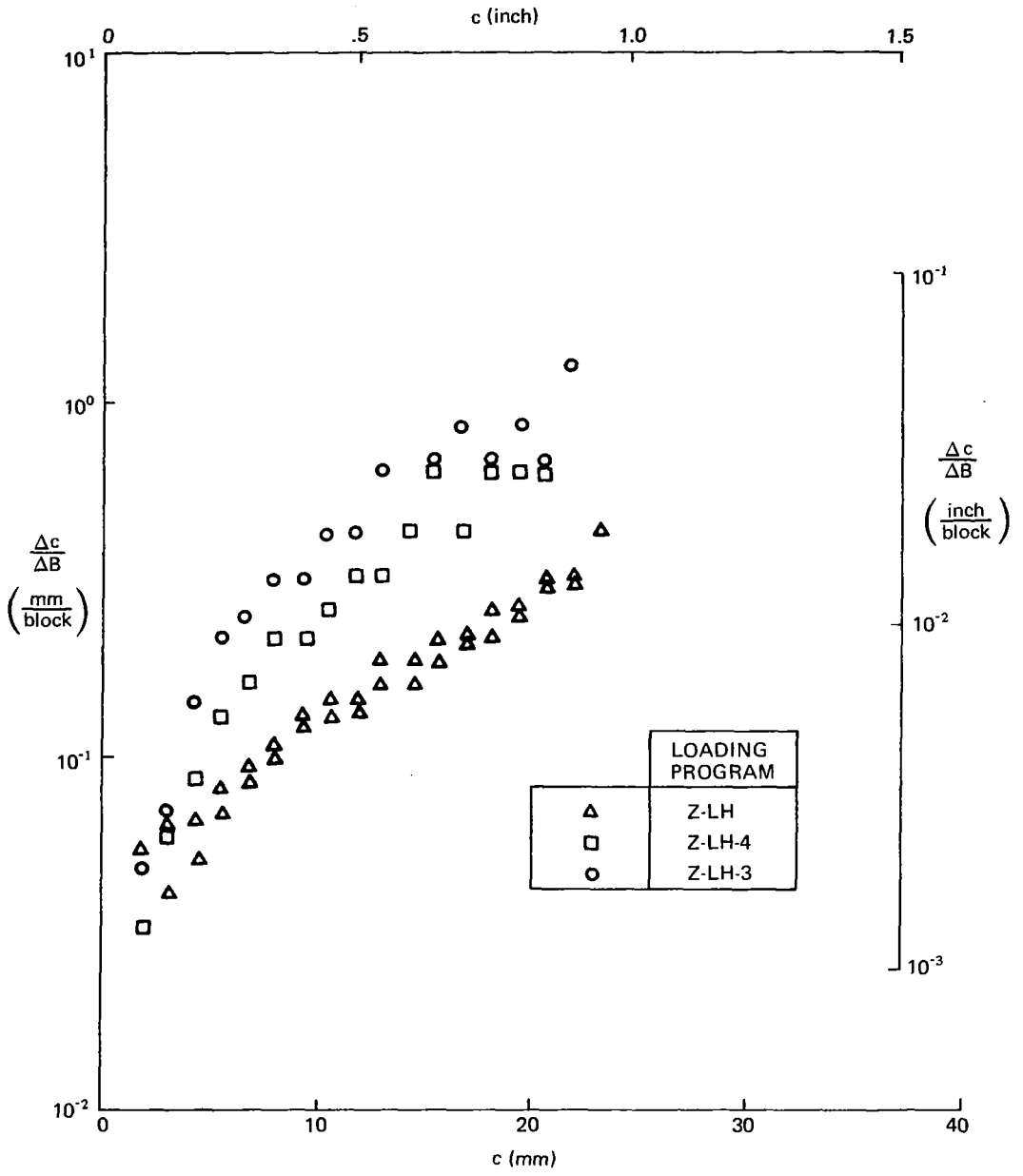

Figure 14.- Variation of fatigue crack growth rate with c. Corner-flaw specimens. Loading programs Z-LH, Z-LH-3, and Z-LH-4. Beta-processed. Longitudinal grain.